Acta Mech Sin (2010) 26:391–399
DOI 10.1007/s10409-010-0343-6

RESEARCH PAPER

Heat transport mechanisms of low Mach number turbulent channel flow with spanwise wall oscillation

Jian Fang · Li-Peng Lu · Liang Shao

Received: 16 January 2009 / Revised: 27 September 2009 / Accepted: 30 September 2009 / Published online: 25 April 2010

Abstract Large eddy simulation (LES) of low Mach number compressible turbulent channel flow with spanwise wall oscillation (SWO) is carried out. The flow field is analyzed with emphases laid on the heat transport as well as its relation with momentum transport. When turbulent coherent structures are suppressed by SWO, the turbulent transports are significantly changed, however the momentum and heat transports change in the same manner, which gives the evidence of inherently consistent transport mechanisms between momentum and heat in turbulent boundary layers. The Reynolds analogies of all the flow cases are quite good, which confirms again the fact that the transport mechanisms of momentum and heat are consistent, which gives theoretical support for controlling the wall heat flux control by using the drag reducing techniques.

Keywords Large eddy simulation · Turbulent heat transport · Wall heat flux · Spanwise wall oscillation

1 Introduction

The aerodynamic heating will cause a series of problems such as increasing thermal loading, reducing mechanical performances of vehicle's materials, and increasing infrared radiation. These problems will be more serious in turbulent flow due to the increase of surface temperature and heat flux. Thus, it is necessary to study the turbulent heat transport mechanism and search for proper methods to control the wall heat flux (WHF). Since the 1970s, plenty of strategies for drag reducing have been developed practically (riblets, compliant wall, polymer additive, micro-bubbles etc.) and theoretically (active controls, wall oscillation etc.), of which most adopt the method of disturbing the turbulent coherent structures (CS). The simultaneity of drag reduction and WHF reduction as well as the consistent changes between heat transport and momentum transport were also reported in some controlled turbulent flows (riblets [1] and polymer additive [2]). These facts inspire the authors to look into the characters of turbulent heat transport and WHF in turbulent flow when the CS is disturbed by some of above strategies.

In the present study, the spanwise wall oscillation (SWO) is adopted as the control strategy to manipulate the turbulent coherent structures. SWO is an effective drag reducing technique in suppressing turbulence activity. It was first studied in 1992 by Jung et al. [3], who got the continual reductions of drag (40% the maximum), turbulence intensity and generation of coherent structures. After the work of Jung et al. [3], Laadhari et al. [4] carried out experimental research on this issue in water channel, validating the conclusions of Jung et al. [3]. Afterwards, lots of researchers [5–21] have done numerical researches with consistent results as those of Jung et al. [3]. Among them, Orlandi et al. [6], Quadrio et al. [12] and Choi et al. [17] carried out respectively numerical and experimental studies in the pipe flow oscillating around its axis, and the maximum drag reduction of 25% was reached accompanied with some similar results as in channel flows.

SWO, as a large scale control technique, has drawn so much attention in recent decades due to its dramatic effect

The project was supported by Key Subjects of the National Natural Science Foundation of China (10732090), the National Natural Science Foundation of China (50476004), and the 111 Project (B08009).

J. Fang (✉) · L.-P. Lu
National Key Laboratory of Science and Technology on Aero-Engines, School of Jet Propulsion, Beihang University, 100191 Beijing, China
e-mail: fangjian@sjp.buaa.edu.cn

L. Shao
Laboratory of Fluid Mechanics and Acoustics, Ecole Centrale de Lyon, Lyon, France

on drag reduction (the maximum drag reduction of 45% can be reached according to Choi et al. [16]; contrastively, the riblets can only reach the level of 10%) as well as its connection with dynamical mechanisms of self-sustain and regeneration process of turbulence. So far as the authors know, the fluids in published researches are all incompressible and thermal field has not been widely studied.

To study heat transport in the controlled turbulent flows, large eddy simulation (LES) of low Mach number compressible turbulent channel flow with SWO is carried out. The reliability of LES method for simulating such problems was sufficiently validated [22], and the consistent changes between streamwise velocity fluctuation and temperature fluctuation, between momentum transport and heat transport as well as between velocity streaks and temperature streaks under the influence of SWO were observed [22]. Therefore, in the present paper, the turbulent channel flows with and without controls are further analyzed with emphases laid on the turbulent heat transport mechanism, especially on its relation with the momentum transport with a view to explain the observed simultaneous changes of momentum transport and heat transport.

2 Methodologies

2.1 Numerical issues

The following three dimensional unsteady compressible Favre-filtered Navier-Stokes equations are numerically solved.

$$\frac{\partial \bar{\rho}}{\partial t} + \frac{\partial \bar{\rho}\tilde{u}_j}{\partial x_j} = 0, \tag{1}$$

$$\frac{\partial \bar{\rho}\tilde{u}_i}{\partial t} + \frac{\partial \bar{\rho}\tilde{u}_i\tilde{u}_j}{\partial x_j} = -\frac{\partial \bar{p}}{\partial x_j} + \frac{\partial \tilde{\sigma}_{ij}}{\partial x_j} - \frac{\partial \tau_{ij}}{\partial x_j}, \tag{2}$$

$$\frac{\partial \overline{\rho}\tilde{E}}{\partial t} + \frac{\partial \left(\overline{\rho}\tilde{E} + \overline{p}\right)\tilde{u}_j}{\partial x_j} = -\frac{\partial}{\partial x_j}\left(\tilde{q}_j + \frac{1}{(\gamma-1)Ma^2}Q_j\right) + \frac{\partial}{\partial x_j}\tilde{u}_i\left(\tilde{\sigma}_{ij} - \tau_{ij}\right), \tag{3}$$

where

$$\tilde{E} = C_V\tilde{T} + \frac{1}{2}\tilde{u_i}\tilde{u_i},$$

$$\tilde{q}_j = -\tilde{k}\frac{\partial \tilde{T}}{\partial x_j},$$

$$\tilde{\sigma}_{ij} = \tilde{\mu}\left(\frac{\partial \tilde{u}_i}{\partial x_j} + \frac{\partial \tilde{u}_j}{\partial x_i} - \frac{2}{3}\delta_{ij}\frac{\partial \tilde{u}_k}{\partial x_k}\right).$$

The residual sub-grid stresses $\tau_{ij} = \rho(\widetilde{u_iu_j} - \overline{u}_i\overline{u}_j)$ and sub-grid heat flux $Q_j = \overline{\rho}(\widetilde{u_jT} - \tilde{u}_j\tilde{T})$ are modeled by using dynamic SGS model.

$$\tau_{ij} - \frac{\delta_{ij}}{3}\tau_{kk} = -C2\overline{\rho}\Delta^2\left|\tilde{S}\right|\left(\tilde{S}_{ij} - \frac{\delta_{ij}}{3}\tilde{S}_{kk}\right), \tag{4}$$

$$\tau_{kk} = C_I 2\overline{\rho}\Delta^2\tilde{S}^2, \tag{5}$$

$$Q_j = -\frac{\overline{\rho}\nu_T}{Pr_T}\frac{\partial \tilde{T}}{\partial x_j} = -C\frac{\Delta^2\overline{\rho}\left|\tilde{S}\right|}{Pr_T}\frac{\partial \tilde{T}}{\partial x_j}, \tag{6}$$

where the coefficients C, C_I and Pr_T are calculated dynamically with the formulas:

$$C_I = \frac{1}{2\Delta^2}\frac{\langle L_{kk}\rangle}{\left\langle \widehat{\overline{\rho}}\alpha^2\widehat{\tilde{S}}^2 - \widehat{\overline{\rho}\tilde{S}}^2\right\rangle},$$

$$C = \frac{\left\langle\left(L_{ij} - \frac{\delta_{ij}}{3}\right)M_{ij}\right\rangle}{\langle M_{kl}M_{kl}\rangle}, \tag{7}$$

$$Pr_T = \frac{C\langle T_kT_k\rangle}{\langle K_jT_j\rangle}.$$

The details of the symbols and modeling can be found in the work of Martin et al. [23].

The finite volume method is employed to discretize the equations, and the artificial dissipation is incorporated to stabilize the computation. The convectional fluxes are calculated with 4-order central scheme in skew-symmetric form [24], the diffusive fluxes are calculated with 2-order central scheme, and the classic 3-order 3-stage Rung–Kutta method is adopted for time integral. The computation and flow conditions are set as $Re = 3000$ (based on bulk velocity and the half-high of the channel; the corresponding friction Reynolds number: $Re\tau \approx 180$); $Ma = 0.5$ (based on bulk velocity and velocity of sound at wall); the size of the computation domain is $4\pi h$ in streamwise, $2h$ in normal and $4\pi h/3$ in spanwise; the number of grids is $64 \times 64 \times 64$. The mesh spacing is uniform streamwise and spanwise, and stretched in the normal direction. The boundary conditions are periodic in the stream and span directions with isothermal no-slip condition at walls.

Because of the weak compressibility of flows, we compare our results with those from incompressible DNS of Kim, Moin and Moser (KMM 1987) [25] for similar Reynolds number for calibration. The comparisons of mean velocity profiles and Reynolds stresses are plotted in Fig. 1.

2.2 Summary of SWO

According to the former researches, the spanwise wall is assumed to oscillate in a sinusoidal way:

$$W_{\text{wall}} = W_{\text{m}}\sin\left(\frac{2\pi}{T_{\text{osc}}}t\right), \tag{8}$$

where W_{m} is the amplitude of the wall oscillating velocity; T_{osc} is the period of the oscillation. The wall temperature keeps constant, and uniform streamwise body force is

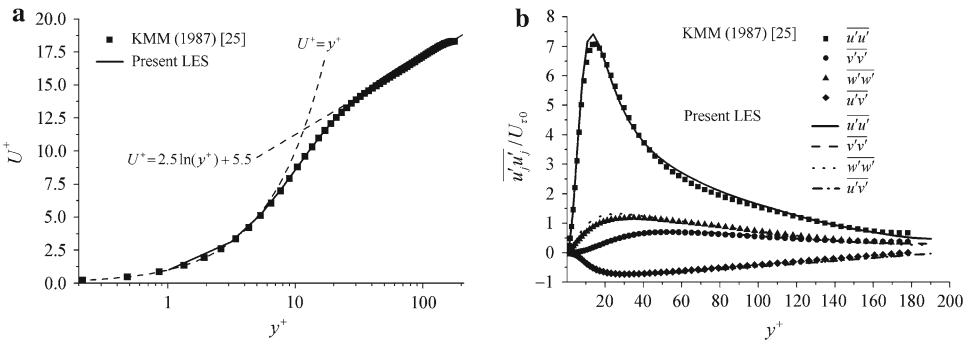

Fig. 1 Comparisons with DNS of KMM (1987) [25]. **a** Mean velocity and **b** Reynolds stresses

Table 1 Parameters of wall oscillating

Case	T^+_{osc}	W^+_{m}	D^+_{m}
C0	Unperturbed channel		
C1	104.1	6.35	204.4
C2	104.1	12.70	408.8
C3	110.4	19.05	649.2

imposed to keep the mass flux to be a constant which equals to that in the fixed channel flow.

Four flow cases including unperturbed channel flow are simulated. The oscillating parameters are listed in Table 1.

In Table 1, Case C0 is the unperturbed fixed-wall channel; D_{m} is the peak to peak displacement of the wall; "+" stands for the variable in wall scale (unless otherwise noted the friction velocity used for nondimensionalization is that of the unperturbed channel flow C0); Case C1 is the same as the best drag-reduction case of Jung et al. [3].

With the spanwise oscillation of wall, the generation of coherent structure is suppressed (as showed in Fig. 2) and the wall stresses (streamwise) are remarkably reduced (as showed in Fig. 3). The WHF is oscillatory (as showed in Fig. 4) with time, due to unsteady dissipation of the periodical spanwise Stokes shear layer. The turbulent transports of momentum ($\overline{u'v'}$) and heart ($\overline{t'v'}$) are significantly suppressed by SWO, as plotted in Fig. 5.

The details of the statistical results, the validation of the drag reduction data and the analyses can be found in Fang et al. [22].

The simultaneous reductions of momentum transport and heat transport indicate the transport mechanisms of momentum and heat are possibly the same. To have deeper insight into the transport mechanisms, especially into the relation between momentum transport and heat transport, the flow fields of both natural and controlled turbulent flows are analyzed. The instantaneous flow fields are investigated to study the coherence between the turbulent motions and the transports; the quadrant contribution is investigated to further study the changes of the transports characteristics, and the Reynolds analogy is also evaluated.

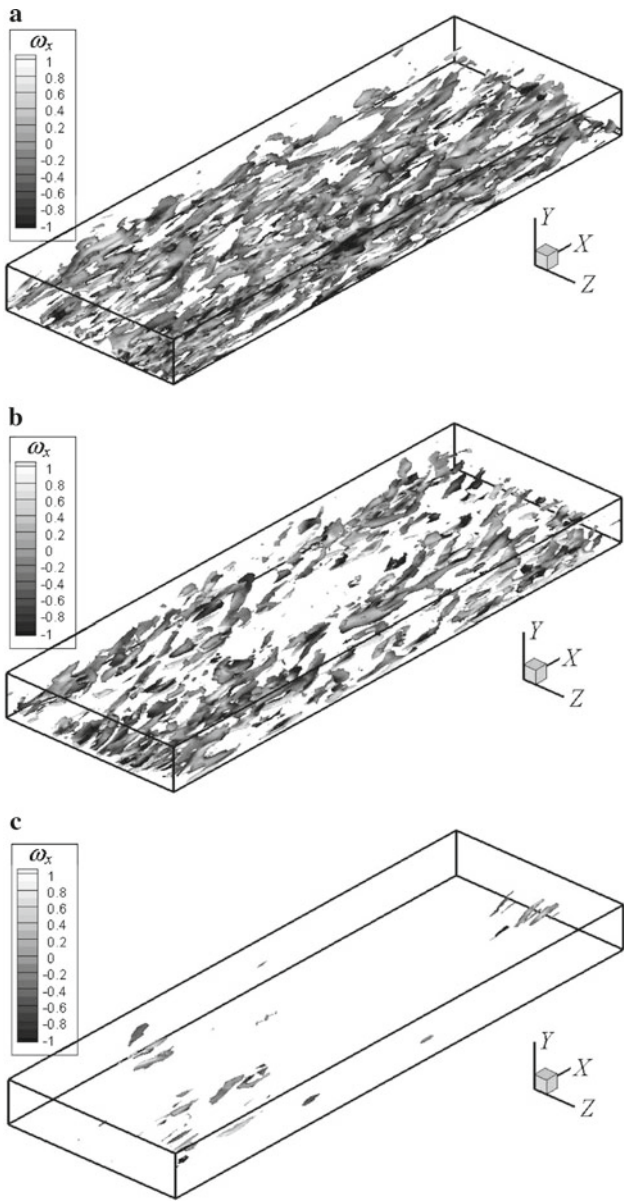

Fig. 2 Evolution of coherent structures of Case C1 (isosurface of λ_2 and colored with streamwise vorticity). **a** $T^+ = 0$, **b** $T^+ = 400$, **c** $T^+ = 825$

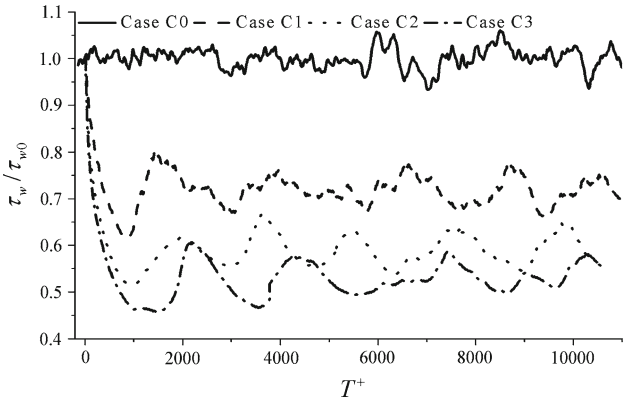

Fig. 3 Time variation of the drag ratio

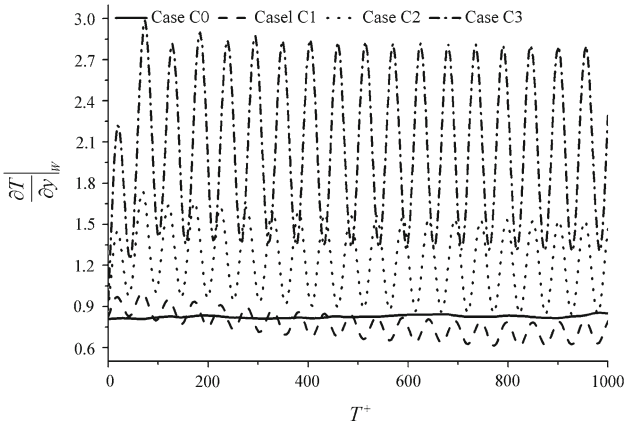

Fig. 4 Time variation of the wall heat flux

3 Results and discussions

3.1 Transport process

To investigate the transport process, the instantaneous flow field is analyzed.

For unperturbed channel turbulence (Case C0), the distributions of fluctuant velocity vectors along with streamwise velocity fluctuation and temperature fluctuation at an arbitrary moment and a $(y-z)$ plane are plotted in Fig. 6.

As we know, the dominant turbulent motion in the turbulent boundary layer is the quasi-streamwise vortex, which induces significant transport effect in the turbulent boundary layer. The quasi-streamwise vortexes can be recognized clearly from the vectors in Fig. 6 (showed in the black circle). The patterns of streamwise velocity and temperature are similar to each other, especially in the near wall region ($y < 0.2$). However, in the outer region, the temperature fluctuation is less active than streamwise velocity fluctuation, which is due to the different mean temperature and streamwise velocity profiles: the mean temperature gradient is much smaller than the mean streamwise velocity gradient in the outer region [22]. How the difference between the streamwise velocity profile and temperature profile influences the relation between velocity and temperature fluctuations statistics and the relation between transports of momentum and heat are discussed in Fang and Lu [22].

With further analyses of the flow field, the high-low velocity regions and high-low temperature regions in the wall region are both distributed alternately in spanwise, which is consistent with the alternate distribution of quasi-streamwise vortexes. The connection of turbulent motions with contour of streamwise velocity as well as with contour of temperature can be concluded as follows:

The downwash sweep motion transfers the high speed and high temperature fluids simultaneously from the outer region to the near-wall region, which increases the velocity and temperature at the sweep position (red regions in both Fig. 6a and b). The upthrust ejection motion takes the low speed and low temperature fluids simultaneously in the near-wall region to the outer region, which will reduce the velocity and temperature at the ejection position (blue regions in both Fig. 6a and b).

The above effects lead to the exchanges of momentum and heat, or in other words, the transports. It can be deduced that, the mechanisms of transports of momentum and heat in the natural turbulent flow are the same, which are both dominated by the organized turbulent vortical motions.

In case of controlled turbulent flows, since the SWO effectively suppress the turbulent coherent structures and

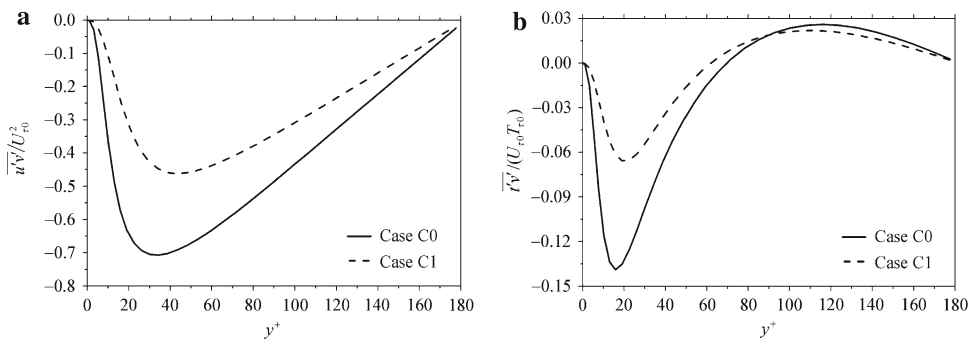

Fig. 5 The turbulent transports. **a** $\overline{u'v'}$ and **b** $\overline{t'v'}$

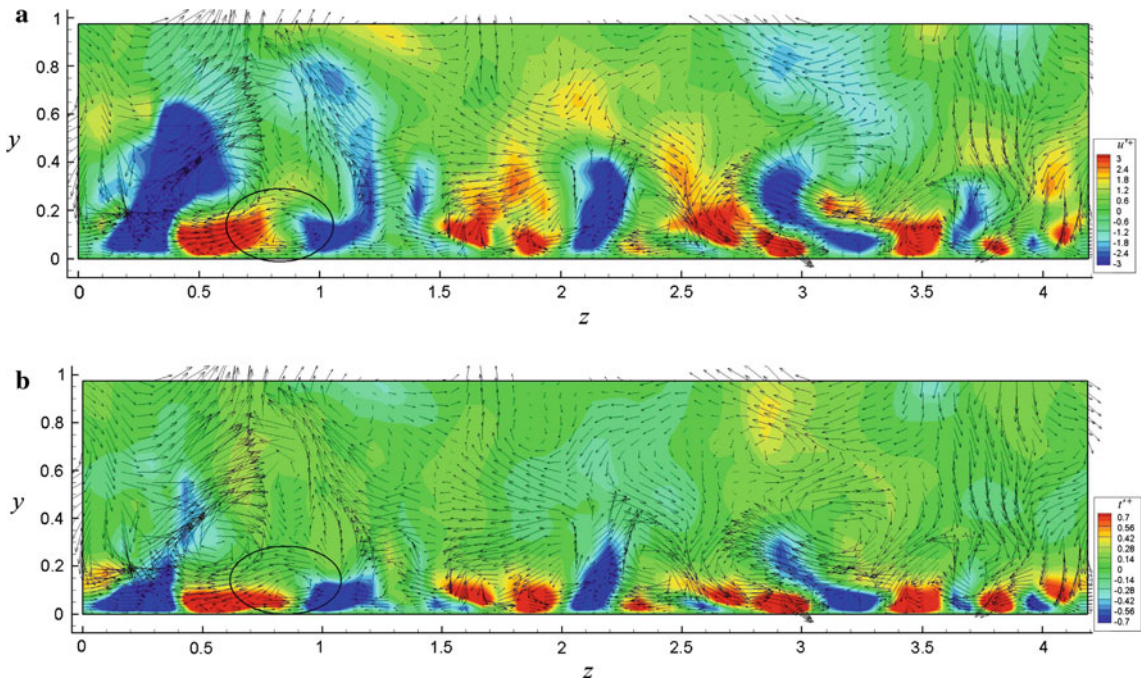

Fig. 6 Velocity vectors (w', v') along with streamwise velocity fluctuations $(u'/U_{\tau 0})$ and temperature fluctuations $(t'/T_{\tau 0})$ in the $(y-z)$ plane for Case C0. **a** Streamwise velocity and **b** temperature

transports, does it change the consistent relation between the transports of momentum and heat? To answer this question, the flow field of Case C1, as plotted in Fig. 7, is analyzed in the same manner.

It should be pointed out that, though the turbulence coherent structures are remarkably suppressed, the quasi-streamwise vortexes can still be recognized (showed in the black circle), continuing to dominate the distributions of streamwise velocity and temperature, thus the transports of momentum and heat.

Compared with the unperturbed channel flow (Fig. 6), the spanwise scales of high-low velocity and high-low temperature regions are increased in the controlled flow, which is consistent with the increase of the width of coherent structures [22]. Based on the analysis of the connections between the streamwise velocity field and the temperature field in turbulent motions, we can figured that, both of the high-low velocity regions and the high-low temperature regions are still closely correlated to the sweeping and ejection of turbulent vortical motions.

The comparative analysis of instantaneous flow fields indicates that though the turbulent coherent structures and transports are dramatically suppressed by SWO, the turbulent transports of momentum and heat are still connected to the turbulent vortical motions, which means that the consistent transport mechanisms of momentum and heat remain unchanged.

3.2 Quadrant analysis

In order to further study the transport characteristics, the quadrant contributions of Reynolds shear stress $\overline{u'v'}$ and normal turbulent heat flux $\overline{t'v'}$ are analyzed.

The quadrant contributions of $\overline{u'v'}$ for both the natural and controlled channel flow are plotted in Fig. 8.

It can be seen from the figure that, the quadrant contributions of $\overline{u'v'}$ are remarkably changed by SWO: the contribution of Q1 increases dramatically and contributions of Q2 and Q4 also increase, but less than Q1. This phenomenon demonstrates the anisotropy of the near wall momentum transport is weakened, which is consistent with the thickening of linear layer and the suppression of near wall organized turbulent motions [22].

The quadrant contributions of $\overline{t'v'}$ for the natural and controlled channel flow are plotted in Fig. 9.

It can be seen that, the change of quadrant contributions of $\overline{t'v'}$ is similar to that of $\overline{u'v'}$: dramatic increase of Q1 contribution and relatively slight increase of Q2 and Q4 contributions, which imply that the anisotropy of heat transport in the near-wall region is also weakened by SWO.

The similar changes of quadrant contributions of $\overline{u'v'}$ and $\overline{t'v'}$ under the influence of SWO demonstrate the inherently consistent transport mechanisms between momentum and heat in turbulent boundary layers, especially in the near-wall region.

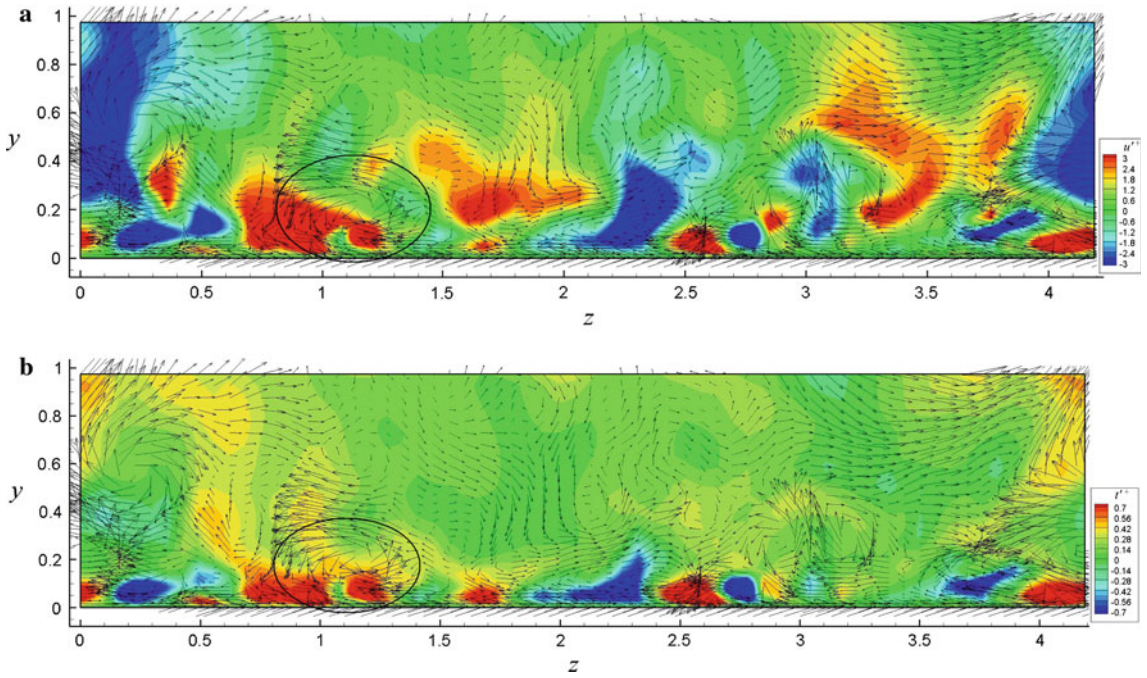

Fig. 7 Velocity vectors (w', v') along with streamwise velocity fluctuations $(u'/U_{\tau 0})$ and temperature fluctuations $(t'/T_{\tau 0})$ in the $(y-z)$ plane for Case C1. **a** Streamwise velocity and **b** temperature

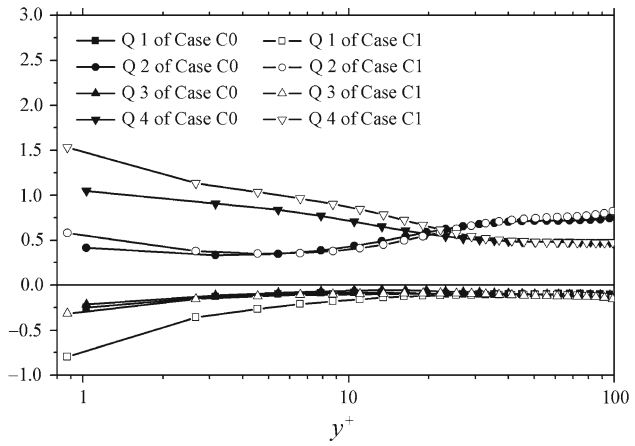

Fig. 8 The quadrant contributions of $\overline{u'v'}$

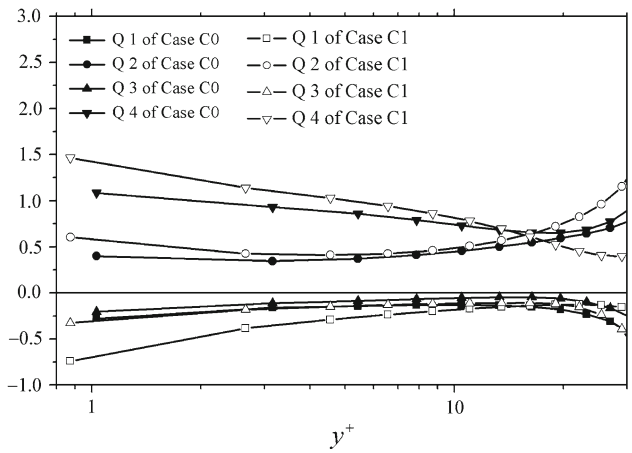

Fig. 9 The quadrant contributions of $\overline{t'v'}$

3.3 Reynolds analogy

According to the analyses above, the mechanisms of momentum transport and heat transport are inherently consistent. Such consistent transport mechanism is a necessary pre-condition for the Reynolds analogy. For further investigation, it's indispensable to evaluate the Reynolds analogy for all the cases.

The friction coefficient Cf and Stanton number St in the channel flow are defined as:

$$Cf = \frac{\mu \cdot \partial u/\partial y}{0.5\rho_b U_b^2}, \tag{9}$$

$$St = \frac{k \cdot \partial T/\partial y}{\rho_b cp(T_b - T_w)U_b}, \tag{10}$$

where the subscript "b" means the bulk averaged value, and the subscript "w" means the wall value.

The instant spanwise distributions of Cf and St of Case C0 at the same moment and streamwise slice as in Fig. 6 are plotted in Fig. 10.

It can be seen that the distributions of Cf and St are highly similar, which clearly shows strong Reynolds analogy.

For the controlled turbulent flow Case C1, the instant spanwise distributions of Cf and St at the same moment and streamwise slice as in Fig. 7 are plotted in Fig. 11.

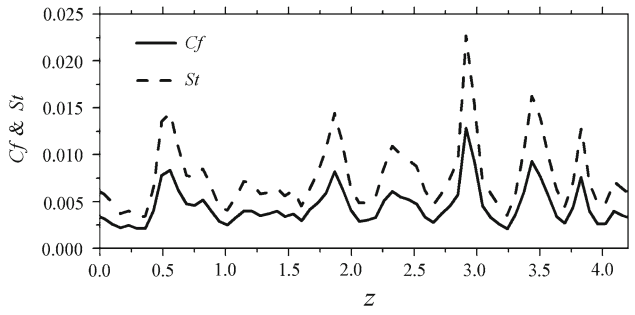

Fig. 10 The instant spanwise distributions of Cf and St of Case C0

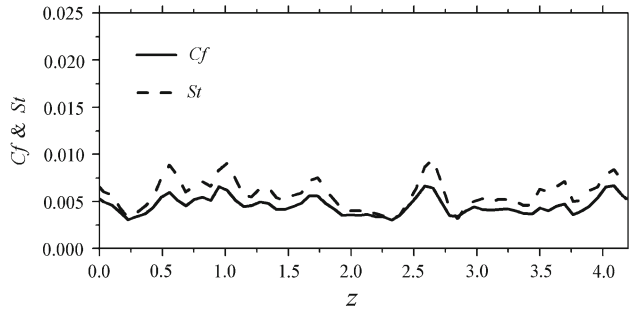

Fig. 11 The instant spanwise distributions of Cf and St of Case C1

The amplitudes of the varieties of Cf and St in Case C1 are reduced obviously by SWO due to the suppression of turbulent intensity, however, the similar distributions between Cf and St still exist in the controlled turbulent flow, and so does the Reynolds analogy. This phenomenon confirms again the consistent transport mechanisms between momentum and heat.

To quantitatively evaluate the Reynolds analogy in all the cases, the correlation of Reynolds analogy C_{RA} is defined as:

$$C_{\mathrm{RA}} = \frac{1}{N}\sum_{N}\frac{(St_i - \overline{St})(Cf_i - \overline{Cf})}{\sqrt{Var_{Cf}\,Var_{St}}}, \tag{11}$$

where Var_{Cf} and Var_{St} stand for the variance of variable Cf and St, respectively. It should be pointed out that $C_{\mathrm{RA}} = 1$ means perfect Reynolds analogy between Cf and St, while $C_{\mathrm{RA}} = 0$ stands for none Reynolds analogy.

To get the statistical values of C_{RA}, the time average should be carried out. For flows with SWO, the time variation of WHF is oscillatory with large amplitude and high frequency (as plotted in Fig. 4) due to the heating effect of the unsteady dissipation caused by oscillatory spanwise Stokes shear layer. To investigate the reason of the oscillation of WHF above, we carry out a simulation of a laminar channel flow with SWO. The comparison of the time spectrum of WHF in Case C1 with that of the laminar channel flow with SWO is plotted in Fig. 12.

It can be seen that, there is lots of spectral energy concentrated around the frequency of SWO in Case C1 and laminar flow. This proves that the large-amplitude, high-frequency oscillation of WHF is attributed to the laminar Stokes flow, not turbulence.

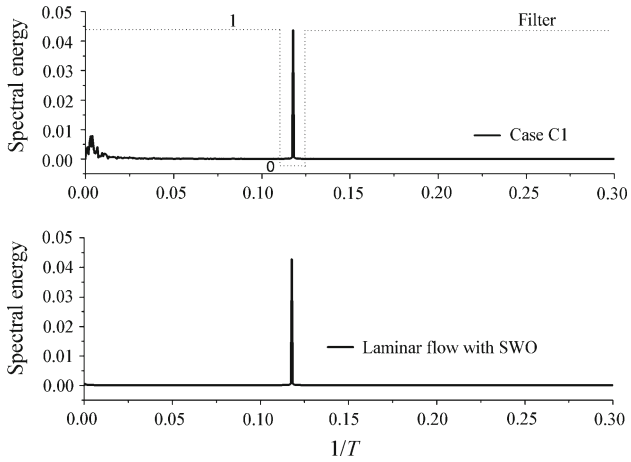

Fig. 12 The time spectrum of WHF of Case C1 and result of the laminar flow with SWO

In the unperturbed turbulent flow, the fluctuations of wall stress and WHF are decided by turbulence. The situation in the flow with SWO is different, the fluctuation of streamwise wall stress $(\partial u/\partial y)$ is still caused by turbulence, while the fluctuation of WHF is attributed to two factors: turbulence and spanwise Stokes shear layer, of which the latter is a laminar flow. Therefore, for flows with SWO, the fluctuation of WHF is artificially divided into "streamwise" and "spanwise" components analogizing to the wall stress. The "streamwise" WHF analogizes to the streamwise wall stress $(\partial u/\partial y)$ which is attributed to the turbulence. The "spanwise" WHF analogizes to the streamwise wall stress $(\partial w/\partial y)$ which is attributed to the Stokes shear layer.

The Reynolds analogy we concern here is the analogy between the streamwise wall stress and the "streamwise" WHF that requires the influence of spanwise Stokes layer to be eliminated. Since the spectrum of WHF caused by the spanwise Stokes shear layer is mostly concentrated around the frequency of SWO and has little interaction with other frequencies, the filter can be designed to remove the spectrum energy around SWO frequency only (the filter is sketched in Fig. 12). Both WHF and wall stress are filtered, and then the filtered values will be used for the statistics of C_{RA}. With the streamwise wall stress (not presented here) filtered, we can see that the present filter has little effect on the turbulence-caused component.

The time variations of filtered St and Cf of Case C1 are plotted in Fig. 13.

It can be seen that, compared with Fig. 4, the filtered WHF is not oscillatory any more, showing that the filter works well. The time variations of filtered Cf and St are very similar to each other, indicating the preservation of Reynolds analogy.

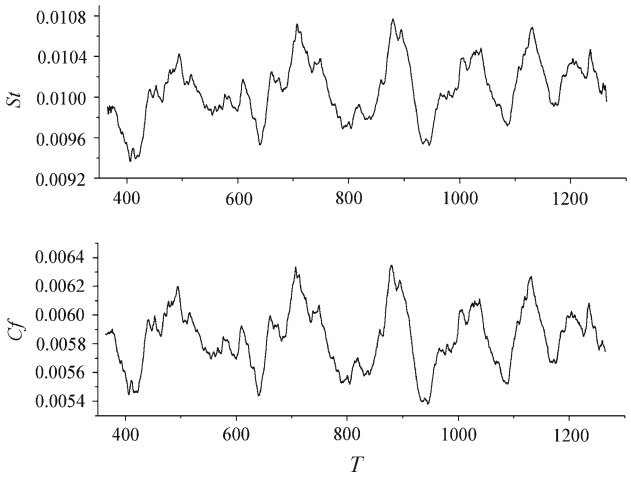

Fig. 13 The time variations of filtered *St* and *Cf*

Table 2 The statistical results of Reynolds analogy

Case	Original			Filtered		
	Cf	*St*	C_{RA}	*Cf*	*St*	C_{RA}
C0	0.0081	0.0011	0.99	0.0081	0.0011	0.99
C1	0.0058	0.010	0.39	0.0058	0.010	0.96
C2	0.0048	0.014	0.11	0.0048	0.014	0.90
C3	0.0043	0.018	0.026	0.0042	0.018	0.90

The statistical results of all the four cases are listed in Table 2. Both the original and the filtered *Cf*, *St* and C_{RA} are calculated.

From Table 2, it can be seen that, the filter has little influence on the mean value of *Cf*, *St* of all the cases and the C_{RA} of Case C0, but it has dramatic influence on the C_{RA} of the controlled cases: without filter the correlation is weak due to the influence of spanwise Stokes layer, and the correlation is even weaker with the increase of the SWO amplitude for obvious reason. However, with the filter, the correlations of all the cases are close to 1, which means that the quality of Reynolds analogy is good and the filter works well. The good Reynolds analogies of all the cases confirm again the inherently consistent transport mechanisms between momentum and heat. In other words, though the turbulent field and transports are changed dramatically by the SWO, the consistent transport mechanisms between momentum and heat remain unchanged all the while.

4 Conclusions

With the large eddy simulation of compressible turbulent channel flows controlled by the spanwise wall oscillation and the analyses of the flow field, the turbulent transport mechanisms of momentum and heat are investigated and some conclusions are reached as follows.

(1) With SWO, the generation of turbulence coherent structure is suppressed, the drag decreases and the intensities of velocity fluctuations and temperature fluctuation as well as the transports of momentum and heat are all suppressed.
(2) In both the natural and controlled turbulent flows, the transports of momentum and heat are consistent with each other, and they are both highly correlated to the turbulent vortical motions; the quadrant contributions of $\overline{u'v'}$ and $\overline{t'v'}$ varies in the same manner too.
(3) The distributions of *Cf* and *St* are distributed similarly to each other for all the cases; the Reynolds analogy persists and the qualities of the analogy are good for all the cases.
(4) The transport mechanisms of momentum and heat are consistent with each other for both unperturbed and controlled turbulent flows. This indicates that it comes from the inherent character of turbulent boundary layers, which gives theoretical support for controlling WHF by using the drag reducing techniques.

It should be motioned that the present study is carried out at low Mach number ($Ma = 0.5$), which means the compressibility is weak. According to the researches of Coleman et al. [26,27] and Ringuette et al. [28], the turbulence statistics and turbulent coherent structures in moderate Mach number ($Ma = 3$) channel flows and flat boundary layer flows are similar to those in incompressible flows. It was also mentioned by Morkvoin [29] and Bradshaw [30] that when the mean flow Mach number is less than 5, the influence of compressibility on turbulent structure can be neglected. Therefore, it can be concluded as follows: in moderate Mach number flows, the turbulent transport characteristics are consistent with those in low-Mach number flows, and the present conclusion will also be valid in this sense. However, in order to study the influence of Mach number on the transports, further investigation into the supersonic and hypersonic flows needs to be carried out.

Acknowledgements The authors are grateful to Dr. Ye Jian for offering the original LES codes and Ms. Fang Juan for her generous help.

References

1. Stalio, E., Nobile, E.: Direct numerical simulation of heat transfer over ribles. Int. J. Heat Fluid Flow **24**, 356–371 (2003)
2. Li, F.C., Kawaguchi, Y.: Investigation on the characteristics of turbulence transport for momentum and heat in a drag-reducing surfactant solution flow. Phys. Fluids **16**(9), 3281–3295 (2004)

3. Jung, W.J., Mangiavacchi, N., Akhavan, R.: Suppression of turbulence in wall-bounded flows by high-frequency spanwise oscillations. Phys. Fluids A **4**(8), 1605–1607 (1992)
4. Laadhari, F., Skandaji, L., Morel, R.: Turbulence reduction in a boundary layer by a local spanwise oscillating surface. Phys. Fluids **6**(10), 3218–3220 (1994)
5. Baron, A., Quadrio, M.: Turbulent drag reduction by spanwise wall oscillations. Appl. Sci. Res. **55**(4), 311–326 (1995)
6. Orlandi, P., Fatica, M.: Direct simulations of turbulent flow in a pipe rotating about its axis. J. Fluid Mech. **343**, 43–72 (1997)
7. Dhanak, M.R., Si, C.: On reduction of turbulent wall friction through spanwise wall oscillations. J. Fluid Mech. **383**, 175–195 (1999)
8. Quadrio, M., Sibilla, S.: Numerical simulation of turbulent flow in a pipe oscillating around its axis. J. Fluid Mech. **424**, 217–241 (2000)
9. Choi, J.I., Xu, C.X., Sung, H.J.: Drag reduction by spanwise wall oscillation in wall-bounded turbulent flows. AIAA J. **40**(5), 842–850 (2002)
10. Huang, X., Xu, C., Cui, G.X., et al.: The influence of spanwise wall oscillation on the transportation of Reynolds stress. In: Proceedings of 2003' Fluid Mechanics Youth Workshop, pp. 206–211. Xi'an, Shaanxi, China, 23–25 November, 2003
11. Huang, W., Xu, C.X., Cui, G.X., et al.: Mechanism of drag reduction by spanwise wall oscillation in turbulent channel flow. Acta Mech. Sin. **36**(1), 24–30 (2004) (in Chinese)
12. Quadrio, M., Ricco, P.: Critical assessment of turbulent drag reduction through spanwise wall oscillations. J. Fluid Mech. **521**, 251–271 (2004)
13. Zhou, D., Ball, K.S.: The Mechanism of turbulent drag reduction by spanwise wall oscillation. In: Proceedings of 42nd AIAA/ASME/SAE/ASEE Joint Propulsion Conference and Exhibit, pp. 1–14. Sacramento California, USA. 9–12 July, 2006
14. Ricco, P., Quadrio, M.: Wall-oscillation conditions for drag reduction in turbulent channel flow. Int. J. Heat Fluid Flow **29**(4), 891–902 (2008)
15. Trujillo, S.M., Bogard, D.G., Ball, K.S.: Turbulent boundary layer drag reduction using an oscillating wall. AIAA Paper: AIAA-1997-1870 (1997)
16. Choi, K.S., DeBisschop, J.R., Clayton, B.R.: Turbulent boundary-layer control by means of spanwise-wall oscillation. AIAA J. **36**(7), 1157–1163 (1998)
17. Choi, K.S., Graham, M.: Drag reduction of turbulent pipe flows by circular-wall oscillation. Phys. Fluid **10**(1), 1–9 (1998)
18. Choi, K.S., Clayton, B.R.: The mechanism of turbulent drag reduction with wall oscillation. Int. J. Heat Fluid Flow **22**, 1–9 (2001)
19. Cicca, G.M.D., Iuso, G., Spazzini, P.G., et al.: Particle image velocimetry investigation of a turbulent boundary layer manipulated by spanwise wall oscillations. J. Fluid Mech. **467**, 41–56 (2002)
20. Iuso, G., Cicca, G.M.D., Onoratob, M., et al.: Velocity streak structure modifications induced by flow manipulation. Phys. Fluids **15**(9), 2602–2612 (2003)
21. Ricco, P., Quadrio, M.: Wall-oscillation conditions for drag reduction in turbulent channel flow. Int. J. Heat Fluid Flow **29**(4), 891–902 (2008)
22. Fang, J., Lu, L., Shao, L.: Large eddy simulation of compressible turbulent channel flow with spanwise wall oscillation. Sci. China Ser. G **52**(8), 1233–1243 (2009)
23. Martin, M.P., Piomelli, U., Candler, G.V.: Subgrid-scale models for compressible large-eddy simulation. Theor. Comput. Fluid Dyn. **13**, 361–376 (2000)
24. Ducros, F., Laporte, F., Souléres, T., et al.: High-order fluxes for conservative skew-symmetric-like scheme in structured meches: application to compressible flows. J. Comput. Phys. **116**, 114–139 (2000)
25. Kim, J., Moin, P., Moser, R.: Turbulence statistics in fully developed channel flow at low Reynolds number. J. Fluid Mech. **177**, 133–166 (1987)
26. Coleman, G.N., Kim, J., Moser, R.D.: A numerical study of turbulent supersonic isothermal-wall channel flow. J. Fluid Mech. **105**, 159–183 (1995)
27. Coleman, G. N.: Direct simulation of isothermal-wall supersonic channel flow. In: Annual Research Briefs, pp. 313–328. Center for Turbulence Research (1993)
28. Ringuette, M., Wu, M., Martin, M.P.: Coherent structures in dns of turbulent boundary layers at Mach 3. J. Fluid Mech. **594**, 59–69 (2008)
29. Morkovin, M.V.: Effects of compressibility on turbulent flows. In: Favre, A. (ed.) Mecanique de la Turbulence, pp. 367–380. CNRS, Paris (1962)
30. Bradshaw, P.: Compressible turbulent shear layers. Annu. Rev. Fluid Mech. **9**, 33–54 (1977)